The use of activated carbon and graphite for the development of lead-acid batteries for hybrid vehicle applications

M. Fernández*, J. Valenciano, F. Trinidad, N. Muñoz

Research & Development Center, Exide Technologies, Avda. Conde de Romanones, 30 E-19200 Azuqueca de Henares, Spain

ABSTRACT

Future vehicle applications require the development of reliable and long life batteries operating under high-rate partial-state-of-charge (HRPSoC) working conditions. This paper updates work carried out to develop spiral wound valve-regulated batteries for vehicles with different hybridisation degrees, ranging from stop–start to mild hybrid applications.

In order to develop a battery that can withstand the hard operating conditions that the work at High Rate Partial-State-of-Charge (HRPSoC) implies, it is necessary to modify the negative AM formulation by using special, additives like carbon and graphite that reduce lead sulphate accumulation during HRPSoC cycling within in the negative plate. Several batches of negative active material (NAM) with the addition of graphites of different types, as well as combinations of graphite and activated carbons, have been made on 6 V 24 Ah Spiral wound modules. Electrical results show a dramatic increase of the charge acceptance at different SoC's that for some combinations approach 200%. On the other hand, on cycle life according to EUCAR Power Assist cycling, values in the range 200,000–220,000 cycles have been obtain in most part of the batch. This represents a capacity turnover of 5000–5500 times the nominal capacity.

The paper is divided into three parts. The first part is devoted to identify the cause of failure of the negative plate on Power Assist Cycle Life, that turned to be the development of high amounts of lead sulphate and its accumulation on the surface of the plate. The second part covers the addition of carbon and graphite of low SSA to NAM and finally the third part is dedicated to the test of additions of medium/high SSA carbon to NAM with the specific objective of trying to implement the supercapacitor effect inside the battery.

© 2010 Elsevier B.V. All rights reserved.

1. Introduction

The already announced legislations on the reduction of vehicles emissions and fuel consumption levels have led in past years to the development of lot of vehicles with different powertrain hybridisation degrees, implementing several hybrid functions to different extents, such as engine stop–start operation, regenerative braking, power boosting on acceleration and various levels of hybrid electric propulsion assist [1]. Depending on the power requirements and vehicle hybridisation degree, several drivetrain and powernet architectures have been proposed [2], with nominal voltages ranging from 14 V to nearly 300 V in automobiles and over 600 V in hybrid buses.

According to the EUCAR Well-to-Wheels Report [3], hybrid vehicles can provide, by 2010, an additional energy reduction of about 15–18% to the results obtained from further developments in energy efficiency and vehicle technology, thus contributing to CO_2 emissions reductions (Kyoto protocol) through reduced fuel consumption. Hybrid vehicles, either with conventional internal combustion engines in the short-medium term, or with a fuel cell as energy generation device, need a battery to store energy generated during cruising periods and regenerative braking. This energy would then be required for vehicle starting and acceleration (booster), besides keeping all consumers working during vehicle stops.

No battery system alone represents up to date a solution, in terms of energy/power performance, life and cost goals, industrial development and recycling facilities, to cope with the stringent performance and cost demands of car manufacturers [4]. Different electrochemical systems have been installed either in commercial hybrid vehicles or in demonstration prototypes: the Toyota Prius, Honda Insight or Ford Escape, with high voltage Ni-MH batteries, the Citröen C3 with stop–start function and AGM VRLA 12 V battery, and the Nissan Tino with a Li-ion 346 V battery [5].

Efficient energy management in vehicles with such functions demands the development of batteries with improved charge

* Corresponding author. Tel.: +34 949 263316; fax: +34 949 262560.
E-mail addresses: melchor.fernandez@eu.exide.com (M. Fernández), jesus.valenciano@eu.exide.com (J. Valenciano), francisco.trinidad@eu.exide.com (F. Trinidad), nuria.munoz@eu.exide.com (N. Muñoz).

Table 1
Experimental matrix and parameter design.

No. batch	Positive plates		Negative plates				
	Grid thickness (mm)	PAM wet density (g cm^{-3})	Grid thickness (mm)	NAM wet density (g cm^{-3})	Organic expander content (%)	Carbon content (%)	Inorganic additive (%)
1	0.9	4.3	0.7	4.3	0.2	0.2% CB	–
2	0.9	4.3	0.7	4.3	0.3	0.2% CB	–
3	0.9	4.3	0.7	4.3	0.2	1.5% EG	–
4	0.9	4.3	0.7	4.3	0.2	1.5% FG	–
5	0.9	4.3	0.7	4.3	0.2	1.5% FG	1.5% PA10
6	0.9	4.0	0.7	4.3	0.2	1.5% EG	–

(1) CB = Standard Carbon Black.
(2) Higher amount of organic expander VAN (0.3% vs. 0.2%).
(3) EG = Expanded Graphite (high SSA = 24 m^2 g^{-1}).
(4) FG = Flake Graphite (low SSA = 9 m^2 g^{-1}).
(5) PA10 = Micro-fiber glass HV.

acceptance as well as longer life under high-rate partial-state-of-charge (HRPSoC) working conditions. Specific demands of each hybridisation degree, as well as cost considerations, have allowed to establish which battery types already in the market or under development fit better to the performance requested [1].

Lead-acid batteries are nowadays extensively used in automotive applications for engine starting, lightning and ignition (SLI) [6]. However, advanced vehicle requirements demand battery working regimes mainly under partial-state-of-charge (PSoC) conditions, that, in the case of flooded batteries, lead to premature capacity loss provoked by electrolyte stratification [7] and active material irreversible sulphation [8]. Changes in the demands on automotive batteries [9] are caused by the increase of on-board power requirements due to the introduction of new features in the vehicles, such as the replacement of mechanical by electrical functions (steer- and brake-by-wire, air conditioning, …) to provide enhanced safety and comfort, as well as of novel functions (stop–start, regenerative braking, etc.) aimed at achieving significant fuel consumption and emission savings.

The increase of electric functions in the vehicles has provoked an evolution of conventional flooded batteries in order to improve power capability (thinner plates with improved corrosion resistant alloys for the grids [10]), life under deep cycle conditions and to reduce water consumption along life.

Valve-regulated lead-acid (VRLA) batteries are also available for vehicles which demand high power linked to a higher capacity throughput due to the higher vehicle energy consumption demands [11]. Moreover, VRLA batteries with spiral wound design provide outstanding performance in terms of power capability and life under different cycling conditions when compared to prismatic designs [12].

VRLA batteries are today the most cost effective solution for short-term low voltage applications (14–42 V powernets), due to their availability, cost and low temperature performance. AGM technology is commonly used, due to the high power capability demanded, the improved life when compared with flooded designs and its intrinsic maintenance free characteristics, as well. However, main drawbacks of VRLA batteries when compared to Ni-MH batteries are their limited charge acceptance, limited capacity turnover

over the battery life under partial-state-of-charge (PSoC) working conditions and reliability under real operation conditions [13]. Trying to deal with this fact is precisely the objective of all the series of tests included in the report.

2. Part 1. Identification of negative plate failure mode

2.1. Experimental work

Six different batches of 6 V 24 Ah high power cylindrical VRLA modules have been manufactured, using different carbon additives in negative active material in combination with different amounts of organic expanders. In addition to highly conductive graphite and with the aim to increase the surface area of the negative active mass, a new inorganic additive (PA10 from H&V) has been tested, in order to examine the influence of this parameter on cycle-life under HRPSoC duty. Finally, two different PAM densities (4.0 g cm^{-3} vs. 4.3 g cm^{-3}) were considered in order to see whether this parameter affects cycle life at HRPSoC. Table 1 details the different process parameters of the prototypes tested:

Once the batteries were assembled and submitted to electrochemical formation process, they were put on electrical testing that included:

- Initial characterisation (C$_{20}$, Reserve capacity and high rate low temperature discharge).
- Power Assist Cycle Life according EUCAR specification [14] (Table 2).

2.1.1. Power Assist Cycle Life

After the initial performance test, at least two samples of every batch were commissioned to perform the Power Assist Cycle Life test as previously described. The main purpose of this test was to determine the influence of the negative plate formulations in the evolution of capacity, voltage and internal resistance under partial-state-of-charge cycling. The profile used for testing is based on the Eucar procedure for HEV applications (see Fig. 1), that has to be repeated 10,000 times (one unit) with the battery at 60% SoC,

Table 2
Initial characterisation.

Tests	Batch # 1 (CB)	Batch # 2 (higher VAN)	Batch # 3 (EG)	Batch # 4 (FG)	Batch # 5 (FG + HV)	Batch # 6 (EG, lower density)
1st reserve capacity (25 A to 5.25 V, min)	32.5	31.5	32.5	33.0	33.0	35.5
2nd reserve capacity (25 A to 5.25 V, min)	34.5	32.0	34.0	35.5	34.5	39.0
Capacity (C$_{20}$) (Ah)	22.9	21.6	22.3	22.4	22.2	24.0
Cold cranking (400 A to 7.2 V, s)	18	21	18	26	22	16
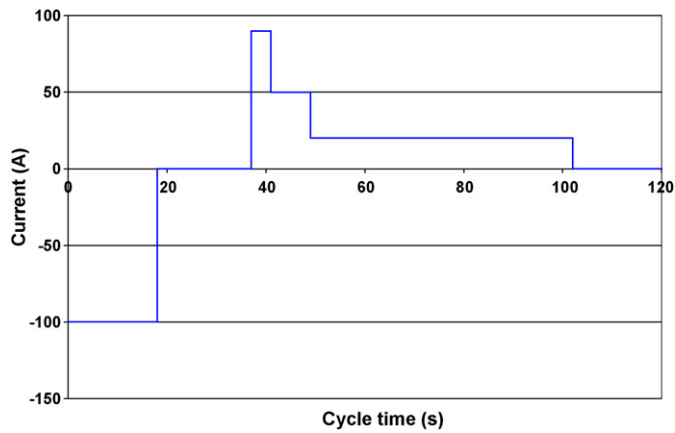
Fig. 1. Power assist microcycle testing conditions.

after which a checking is performed for capacity, weight and internal resistance. An end of discharge voltage of 5 V (per 6 V module) reached along the cycling, or a battery capacity under 50% of initial value was considered as battery failure criteria.
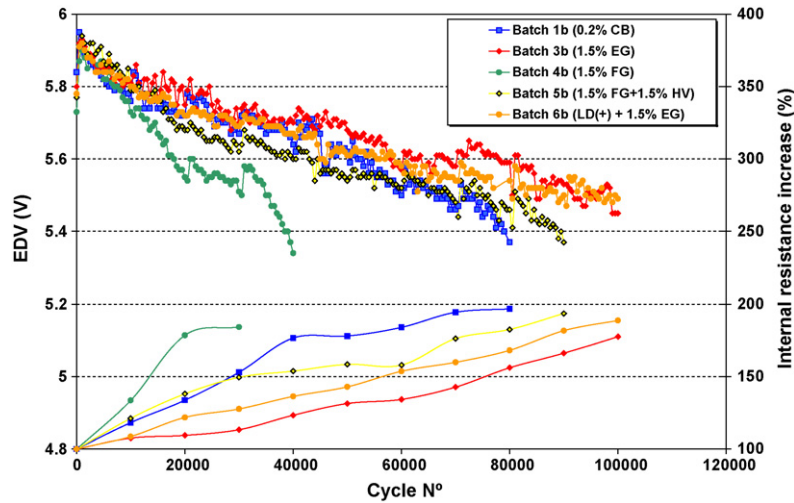
The prototypes were cycled and fan-cooled individually to avoid an excessive increase of temperature. Under these conditions, the temperature measured on the external walls did not exceed 35 °C.

Figs. 2 and 3 show the evolution of the End of Discharge Voltage (EDV), and battery capacity with cycle life. Very high values were obtained, being the formulations that include Expanded Graphite (EG), the ones that achieve higher cycle life. Also the formulation including intermediate paste density in positive AM, showed the highest results.

Battery capacity and End of Discharge Voltage, shows the same trend along life. Internal resistance match also closely the evolution of capacity and EDV (Figs. 2 and 3).

2.1.2. Cadmium readings on power assist cycling

In order to try to investigate in more detail the cause of battery failure, a Power Assist Cycling test with Cadmium electrodes in all cells was performed. This arrangement allows to take separately the voltage of the positive and negative electrode and consequently to observe its evolution on cycling. Results can be seen in Fig. 4. During the discharge step, both plate voltages remain fairly stable, with only a minor decay in the negative plates. On charge, the situation is quite different, because whereas the voltage of the positive plates

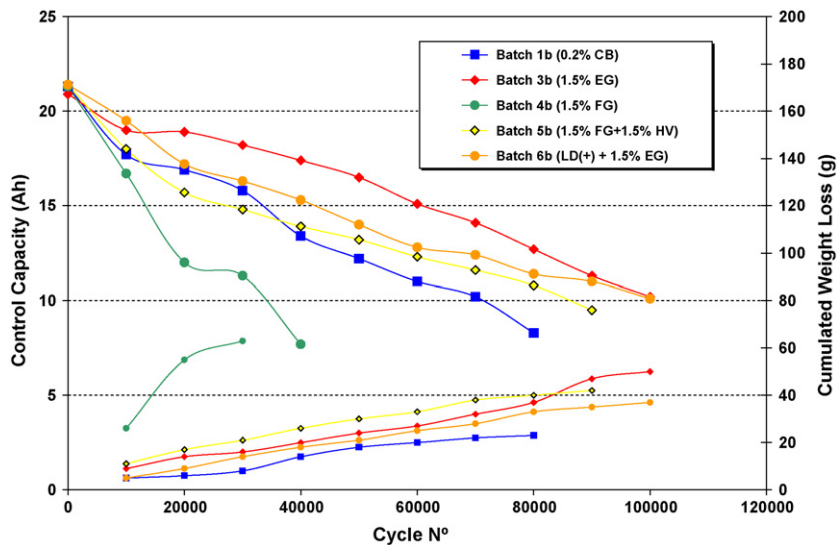**Fig. 2.** End of discharge voltage and electrical resistance on Power Assist Cycle Life.

Fig. 3. Capacity and weight evolution on Power Assist Cycle Life.

Table 3
Physico-chemical analysis after Power Assist Test.

Sample ref.	Positive active material					Negative active material		Power Assist Cycles
	Porosimetry (Hg)		SSA	X-ray Diffraction (% ±4)		Chemical analysis	SSA	
	Porosity (%)	Apparent density (g cm⁻³)	BET (m² g⁻¹)	α-PbO₂	β-PbO₂	PbSO₄ (%)	BET (m² g⁻¹)	
Batch 1 (STD)	53.4	4.25	1.92	9	91	54.2 (top) 50.5 (mid.) 15.6 (bot.)	0.26 (top) 0.30 (mid.) 0.46 (bot.)	110,000
Batch 2 (0.3% VAN)	51.4	4.48	1.83	8	92	53.8 (top) 55.7 (mid.) 20.6 (bot.)	0.29 (top) 0.20 (mid.) 0.34 (bot.)	110,000
Batch 3 (EG)	50.9	4.40	1.72	12	89	39.8 (top) 50.2 (mid.) 14.9 (bot.)	0.43 (top) 0.36 (mid.) 0.52 (bot.)	100,000
Batch 4 (FG)	49.9	4.58	3.4	7	93	71.3 (top) 48.9 (mid.) 23.8 (bot.)	0.40 (top) 0.48 (mid.) 0.61 (bot.)	40,000
Batch 5 (FG + HV)	51.8	4.45	2.2	6	94	54.0 (top) 56.3 (mid.) 16.9 (bot.)	0.31 (top) 0.29 (mid.) 0.40 (bot.)	90,000
Batch 6 (LD + EG)	54.0	3.94	1.78	N.A.	N.A.	47.7 (top) 51.3 (mid.) 13.5 (bot.)	0.38 (top) 0.40 (mid.) 0.54 (bot.)	100,000

N.A.: no analyzed.
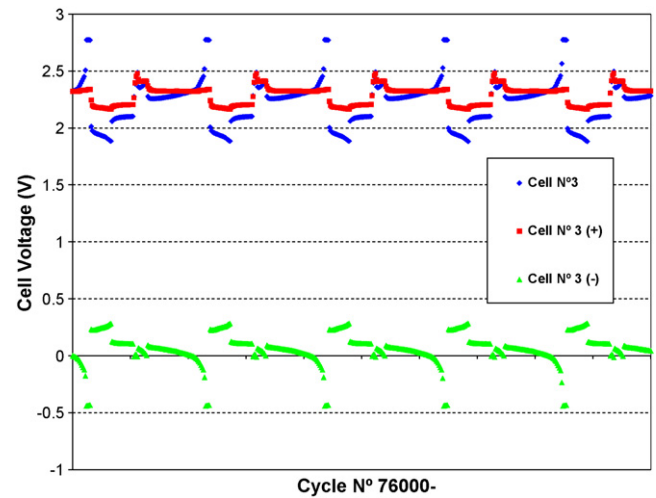
Fig. 4. Cadmium readings on Power Assist Cycle Life.

remain essentially stable with only a minor spike at the beginning, the one of the negative shows a very high polarization at the end of the charging period. This fact provokes a very high charging voltage in the battery, with values approaching 2.8 V clearly deleterious for the electrical performance of the battery. The most deleterious effects of these high charging voltages are corrosion and especially water electrolysis and the consequent dry out of the battery, that finally results in failure.

2.1.3. Teardown and analysis

After failure on cycling, batteries of all groups were torn down for examination and physicochemical analysis of the components. Attached tables reflect the analysis of positive and negative plates. The values of the positive plate shows the general trend that is observed when the battery is submitted to repetitive cycling. The negative plate shows very high levels of lead sulphate in the upper and middle part of the plate, amounting in most cases to more than 50%. These high sulphate values are probably the most important factor that explain the high polarisation levels found in the negative plates at the end of the charging step on Power Assist cycling (Table 3).

2.1.4. Electron Probe Micro Analysis (EPMA) of failed negative plates

In order to have a better knowledge of the possible effects of these high sulphate levels, samples of failed negative plates once completely charged, were cut and submitted to EPMA analysis to look at the sulphate distribution [15]. Samples were taken from the inner, middle and outer part as well as top and bottom of the cylinder. Results are summarized in Figs. 5 and 6, that correspond the first one to the standard batch with not special additive and the second to batch no. 6 with the addition of 1.5% Expanded Graphite. For the standard batch, a dense layer of lead sulphate in the outer part of the plate is clearly seen, whereas with the addition of graphite, lead sulphate is evenly distributed all along the thickness of the plate. The dense layer of sulphate on the surface clearly represents a strong barrier for the diffusion of sulphate ions from the acid, which in turn provokes a strong limitation of the charge and discharge process in the interior of the plate.

2.1.5. Conclusions from part one

From the tests performed in this part of the work, it can be concluded that failure on Power Assist Cycle Life, on batteries without special additives is due to the negative plate, being the specific
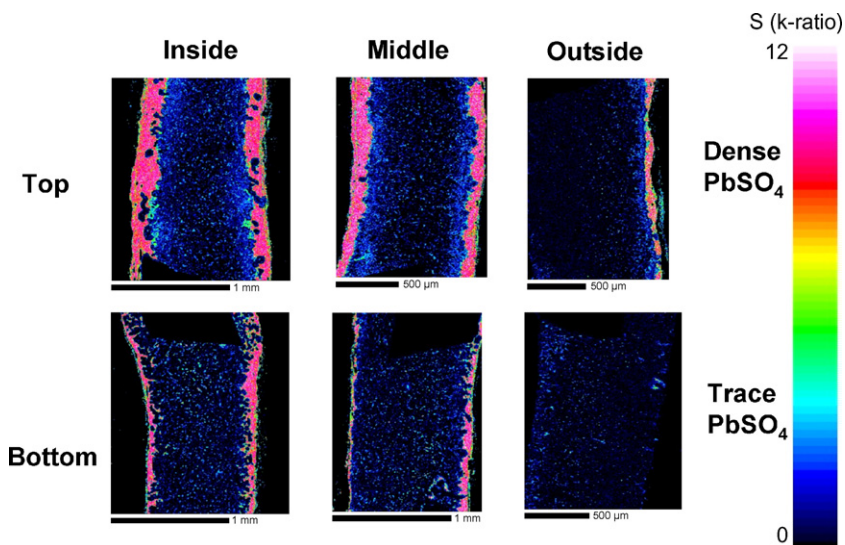
Fig. 5. EPMA analysis of standard batch.

reason the strong accumulation of lead sulphate that develops along cycling. This sulphate accumulates on the surface of the plate, forming a thick and dense layer whose main affect is to make difficult the diffusion of sulphate ions to and from the plate. Small diffusion from the electrolyte, creates acid depletion in the pores of the plate that in turn provokes a significant decrease of the discharge performance of the negative plate. When graphite is added the situation changes. A great amount of lead sulphate is still developed, but instead of being accumulated in a dense layer on the surface, it is evenly distributed all along the thickness of the plate. In this way the negative influence on acid diffusion is strongly decreased and as a consequence its deleterious influence on discharge takes more time to appear and consequently life duration on cycling is markedly increased.

3. Part 2. Tests with low SSA carbon and graphites

Once the cause of failure has been clearly identified and the beneficial influence of graphite in achieving higher cycle lives demonstrated, the next part was dedicated to testing different graphite types, as well as a combination of graphite and conductive carbon black. The purpose of these tests was to study the influence of these additives in charge acceptance and discharge power at different States of a Charge and temperatures, and the influence on Power Assist Cycle Life.

In order to gain a deeper understanding of the way in which carbon and graphite work in the battery, Power Assist Cycles with Cadmium electrode readings, were performed at regular intervals during Power Assist Cycling. Also several modules were taken out of cycling at different stages and torn down to make physicochemical analysis of the components.

The selection of graphite and carbon to be added to the negative mix, was made taking into account the results already obtained in a previous work [15]. Carbon was selected taking as premium consideration the Specific Surface Area, whereas for graphite electrical conductivity is one of the main issues.

3.1. Testing matrix

The following additives have been used in the five batch assembled. It includes three expanded graphite with similar SSA, but different particle size, a synthetic graphite with considerable lower
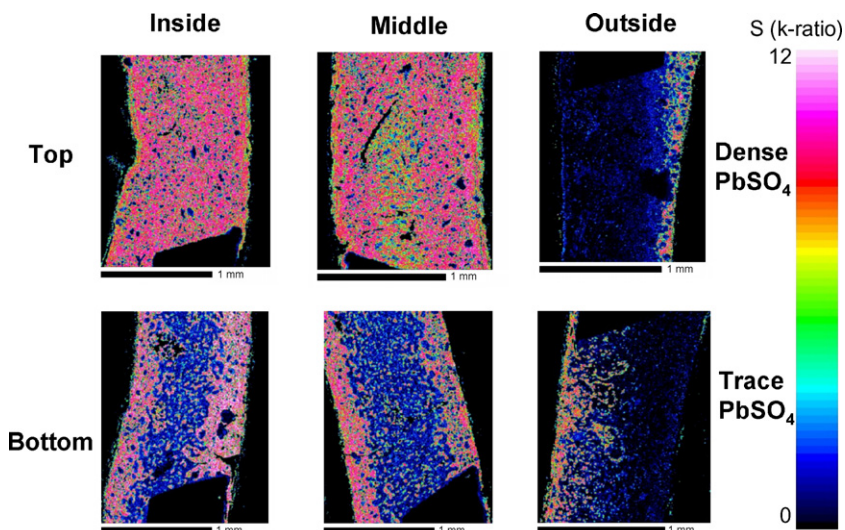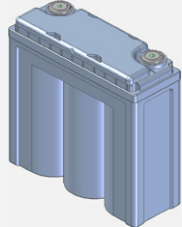

Fig. 6. EPMA analysis of 1.5% expanded graphite batch.

Table 4
Characteristics of carbon compounds.

Carbon compound	Average particle size d50 (μm)	BET specific surface (m² g⁻¹)
Expanded graphite 1 (EG-1)	10	24
Expanded graphite 2 (EG-2)	45	18.2
Expanded graphite 3 (EG-3)	25	20.5
Synthetic graphite (SG)	12	8
Conductive carbon black (CCB)	(27 nm)*	80

Average primary particle size.

Table 5
Experimental Matrix of 6 V 24 Ah Modules.

	Prototype batch
175 × 65 × 190 mm, 4.7 kg	EG-1
	EG-2
	EG-3
	SG
	EG-CCB

SSA, and finally a combination of expanded graphite and low SSA carbon black (Table 4).

The previous additives have been added as shown in Table 5.

3.2. Electrical tests

Once assembled and electrochemically formed, the batteries were submitted to electrical test, that included:

- Initial characterization.
- Charge and discharge power at different SoC's and temperatures.
- Power Assist Cycle Life.
- Teardown and analysis.

3.2.1. Initial characterisation

Values of reserve capacity as well as 20 h capacity are very similar. The same can be said for high rate low temperature discharge, except for synthetic graphite and the combination graphite and carbon for which a moderate decrease is observed (Table 6).

3.2.2. Charge and discharge power

On hybrid vehicle application the power on discharge released by the battery and the charge acceptance power are of great importance. Discharge power because it determines the degree of achievable electrical boosting during the acceleration period and charge acceptance because it fix the degree of utilization of the regenerative braking energy during the deceleration step. In order to simulate the different conditions in which the battery can work in the vehicle, the test is conducted at different SoC's ranging from 20 to 100%, and temperatures between 0 and 40 °C. Also to closely simulate vehicle use, both discharge and charge power are mea-
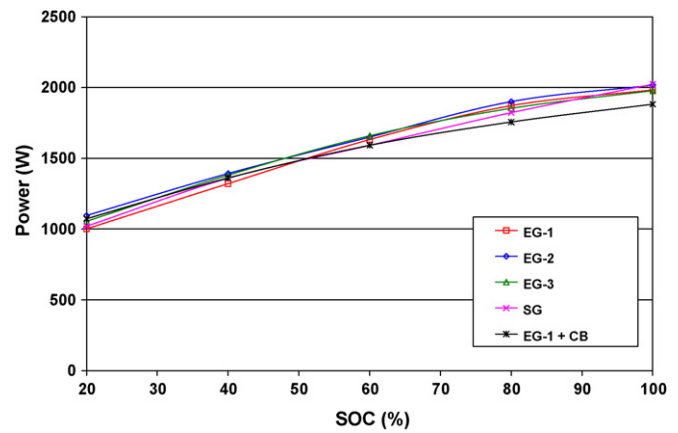

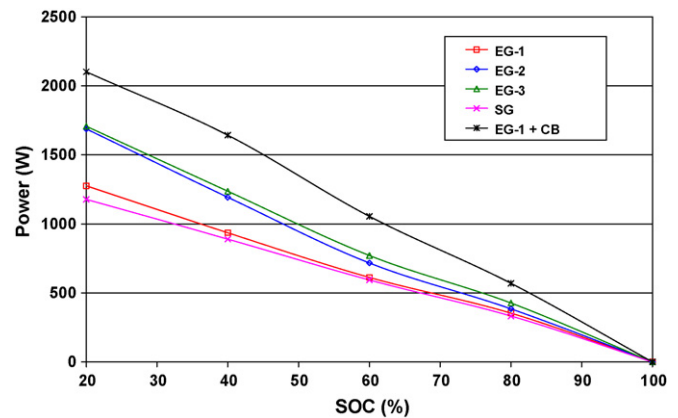**Fig. 7.** Discharge power, 5 V, 10 s, 25 °C.

Fig. 8. Charge acceptance power, 8 V, 5 s, 25 °C.

sured at short times (10 s for discharge and 5 s for charge). Results are summarized in the following graphs (Figs. 7–10).

3.2.2.1. Discharge power. The values are quite similar for all batches at the same temperature. They are heavily dependent on the battery SOC as can be expected, with double value at 100% SoC with respect to 20%. Discharge power shows a heavy dependence with the temperature with increments of 40–60% when going from 0 to 25 and 40 °C.

3.2.2.2. Charge acceptance. The values are strongly dependent on the additive used. This is especially true for the combination Expanded graphite + Conductive carbon black. Comparing with the formulations with only expanded graphite, the increase ranges between 30 and 60% and even higher with respect to synthetic graphite. This clearly shows the strong effect of the Specific Surface Area of the added carbon. Temperature has a strong effect, with increments that amount to more than 200% when going from 0 to 40 °C.
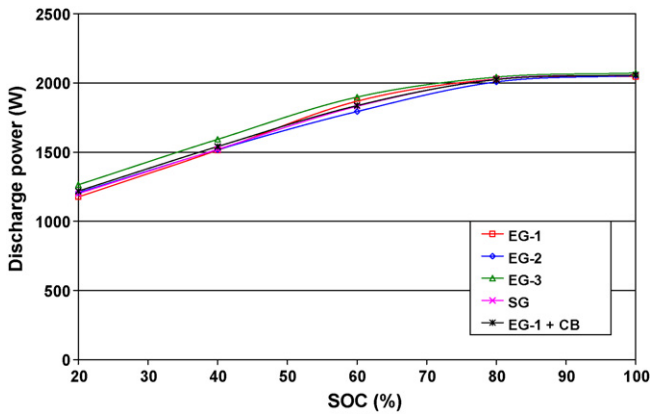
Table 6
Initial characterisation of 6 V 24 Ah modules.

Reference	Weight (kg)	Internal resistance (25 °C, 1 kHz) (mΩ)	C₂₀ (1.2A/5.25 V) (Ah)	Reserve capacity (25A/5.25 V) (min)	HR discharge −18 °C (400 A/3.6 V)	
					$V_{10 s}$ (V)	$D_{3.6 V}$ (s)
EG-1	4.74	2.18 ± 0.05	24.4 ± 0.5	40.9 ± 0.5	4.28 ± 0.03	38 ± 2
EG-2	4.74	2.19 ± 0.03	25.5 ± 0.2	41.3 ± 0.5	4.21 ± 0.01	39 ± 1
EG-3	4.72	2.20 ± 0.04	24.7 ± 0.2	39.6 ± 0.2	4.28 ± 0.02	39 ± 2
SG	4.73	2.23 ± 0.04	24.3 ± 0.3	37.9 ± 1.0	4.16 ± 0.07	31 ± 4
EG-CCB	4.57	2.31 ± 0.07	24.5 ± 0.4	37.4 ± 1.4	4.12 ± 0.04	31 ± 2

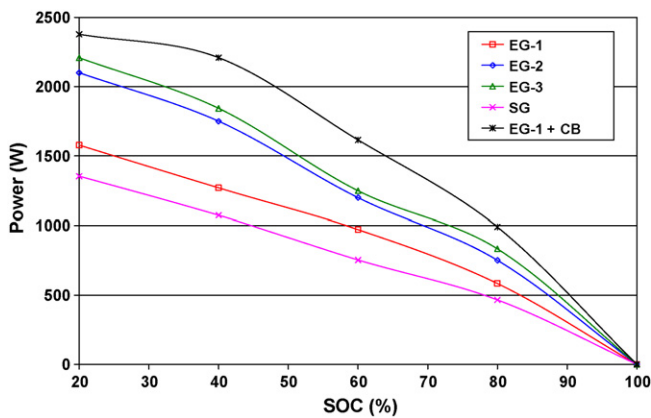**Fig. 9.** Discharge power, 5 V, 10 s, 40 °C.

Fig. 10. Charge acceptance power, 8 V, 5 s, 40 °C.

3.2.3. Power Assist Cycle Life

Once characterised, all batches were submitted to Power Assist Cycling tests in the same conditions as in part 1. The results are shown in Fig. 11.

All the batches achieve lives in excess of 200,000 cycles, which represent a total capacity turnover of between 5000 and 5500 times the nominal capacity. This is a remarkable good result that shows that the battery can approach the life of the vehicle itself making unnecessary any battery replacement during the useful life of the vehicle. No differences are observed between the different additives.
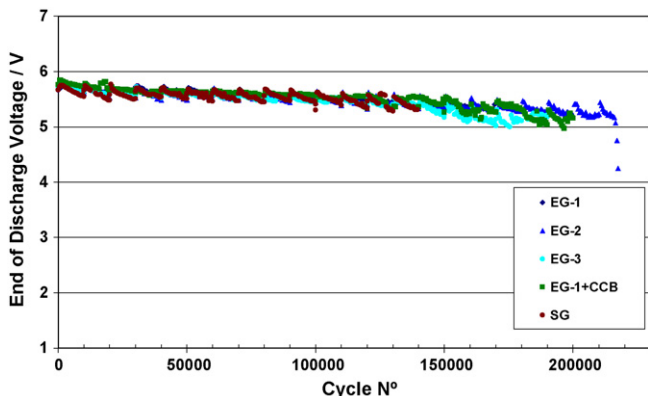

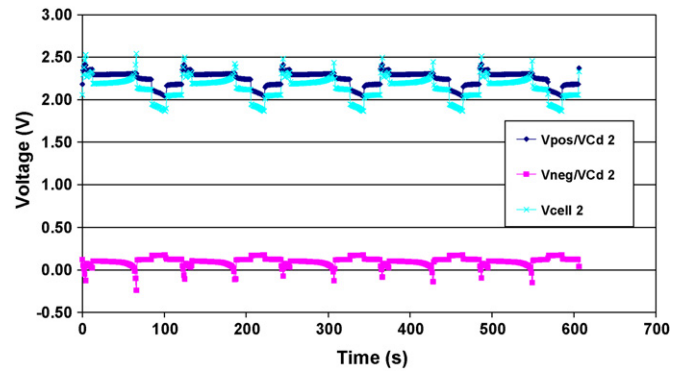**Fig. 11.** Power Assist Cycle Life test, 60% SoC, 2.5% DOD.

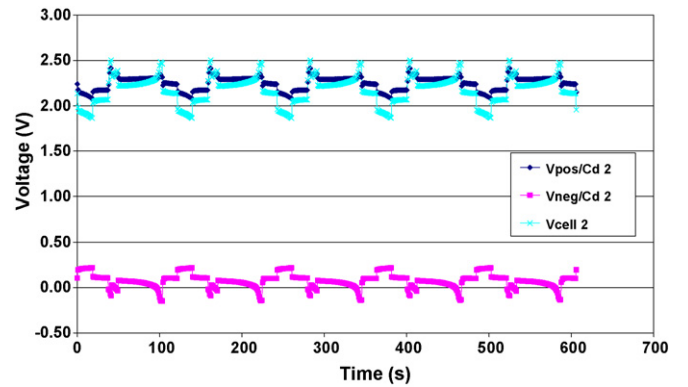**Fig. 12.** Cadmium reference electrode measurement in batch EG-1 (50,000 cycles).

Fig. 13. Cadmium reference electrode measurement in batch EG-1 (100,000 cycles).

3.2.4. Cadmium readings during Power Assist Cycle Life

In order to try to correlate the changes occurring in the negative plate (lead sulphate accumulation, modification of internal structure) with the electrical performance of the battery, a series of Power Assist Cycles were performed, taking during the same the individual voltages of positive and negative plates against a Cadmium reference electrodes. These tests were performed with intervals of 50,000 cycles, this is at 50,000, 100,000 and 150,000 cycles. The evolution will be followed for one batch (EG-1) because it is similar for all batches. It can be seen in Figs. 12–14.

3.2.4.1. Discharge.
On discharge, the same fact already indicated in part 1 was observed, namely some voltage fall in positive plates, whereas the negatives remain essentially flat with no tendency to fall. This tendency is maintained invariably all along cycling.
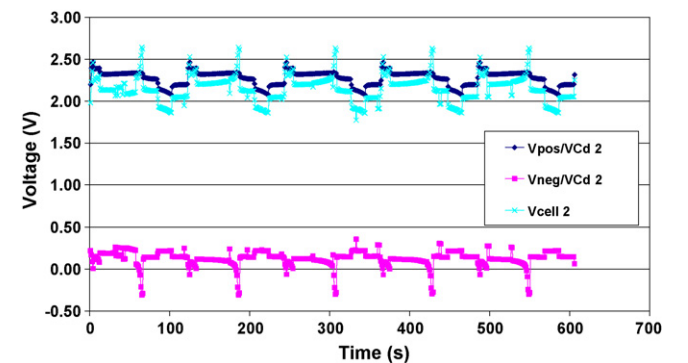

Fig. 14. Cadmium reference electrode measurement in batch EG-1 (150,000 cycles).

Table 7
Physical and chemical characteristics of EG-1 type modules at different ageing degrees.

	Positive active material						Negative active material	
	Chemical analysis	Porosimetry		Specific surface BET ($m^2\,g^{-1}$)	X-ray diffraction (%)		PbSO$_4$ (%)	BET ($m^2\,g^{-1}$)
	PbSO$_4$ (%)	Porosity (%)	Apparent density ($g\,cm^{-3}$)		α-PbO$_2$	β-PbO$_2$		
After characterisation tests	7.5	45.9	4.68	7.80	20	69 (2:7)	8.7	0.79
60,000 cycles	2.2	54.8	4.04	1.33	7	92 (1:13)	15.6 / 5.8	0.73 / 0.77
110,000 cycles	<0.2	54.6	4.03	0.89	5	92 (1:19)	23.3 / 6.4	0.74 / 0.71
200,000 cycles	1.6	55.5	3.90	0.75	3	97 (1:32)	35.0 / 17.2	0.77 / 0.68

3.2.4.2. Charge. On charge also the already mentioned heavy polarisation in the negative plates occurs. The highest polarisation occurs at the end of the low rate charging period (1 C, 54 s), and develops at the very end of this period. Probably the explanation is related with the high polarisation that develops inside the pores of the plate due to a strong increase of the acid concentration provoked for one side for the for the relative high duration of this charging step, and on the other side in the lack of diffusion of the acid from the pores of the plate. This acid diffusion hindrance, is in agreement with the relative high levels of lead sulphate that develops in the negative plates just from relative low number of cycles. For the analysed batch (EG-1) the sulphate levels are 15, 23 and 35% for 50,000, 100,000 and 150,000 cycles.

3.2.5. Teardown and analysis

During and at the end of Power Assist Cycle Life, all the batches were torn down and analysed: Only the results corresponding to batch EG-1 are shown because the evolution is similar for all the groups.

The most remarkable facts include.

Positive plate. A fairly low level of lead sulphate around 2% is observed that does not increase with cycling. Porosity experiments a sharp increase with respect to initial, but afterwards it remain almost constant. Positive plate develops the so-called "coralloid" structure that is characterised by a more open internal structure of the plate.

Negative plate. The most noticeable fact is the already mentioned development of significant amounts of lead sulphate especially in the upper part of the plate. When looking at the data in Table 7 it is clearly seen the steady increase of lead sulphate as cycling progress, amounting at the end of cycling to 35% and 17% for the top and bottom part of the plate.

4. Part 3. Tests to implement supercapacitor effect inside the battery

In mild hybrid vehicle uses the most important properties of the battery are related with its ability to provide power boosting on the acceleration step, as well as the ability to recover as much as possible of regenerative braking energy. Both acceleration boosting and regenerative braking, are characterised by the high amount of power and the short duration of both steps typically of the order of a few seconds. For micro hybrids whose operating voltage is typically 12 V regenerative braking power in the range 2–4 kW can be found, which represents charging currents as high as 300 A. The lead-acid battery is not the optimum component to deal with such high currents due to the very strong polarisation that they provoke in the battery. Due to this, substantial amounts of energy are lost and what is even more important deleterious effects to the life of the battery occur. Amongst them are corro-

sion and above all water consumption that finally result in life limitation.

Supercapacitors due to its basic working principle, are adequate to dealt with these high and short duration currents. In fact because their working principle implies just charge separation they can absorb and release very high bursts of power. The battery and supercap would be complementary [16], taking the supercap the initial 1–2 s power depending on its capacitance and the battery the rest.

Supercapacitor effect is based in the use of very high surface area materials, that can provide a very high capacitance values of the order of hundred or thousand of farads. These materials are generally based in carbon, mainly on the activated carbon group with SSA values in the range 200–2000 $m^2\,g^{-1}$. With this kind of materials, values of capacitance in the range of 16–160 farads g^{-1} of activated carbon can be obtained.

4.1. Supercapacitor implementation theoretical considerations

In any electrolytic aqueous electrolyte capacitor, the equivalent total faradic capacity, is the combination in series of the anode and cathode capacitors, that mathematically is given by the formula

$$1/C\,\text{equivalent} = 1/C\,\text{anode} + 1/\text{cathode}$$

The formula clearly indicates that for achieving the maximum possible equivalent capacitance it is necessary that both anode and cathode faradic capacitances must be equal. Any other combination results in a capacitance lower than the highest one.

According to the previous consideration, it is necessary to make both anodic and cathodic faradic capacitance values the most similar to each other. The configuration wanted to be implemented is an asymmetric capacitor in which the anode capacitance is provided by the positive plate as it is, and the cathode by the modified negative plate by adding to it high Specific Surface Area additives.

Positive plate. A small literature review has been made to get a reliable estimation of the faradic capacitance of this plate on its standard configuration. The values found in [17] expressed in $\mu F\,cm^{-2}$ are in the range of 40–60 $\mu F\,cm^{-2}$, that for a standard plate represent a theoretical value between 150 and 225 Farads. Practical achievable values are not so high due to different reasons like for instance the real accessibility of the electrolyte to all the internal SSA that depends on the pore size distribution. Real achievable capacity is around one-fifth of the previous figure, which results in a value of around 30–45 Farads plate^{-1}.

Negative plate. Faradaic capacitance values found in the literature, are around 17 $\mu F\,cm^{-2}$, which for a standard plate represents a capacity of around 7 Farads, a value between 20 and 30 times lower than the one of the positive. The main reasons are the low specific surface area (around 10 times lower), and also that specific capacitance per unit area is lower on the negative plate. According

Table 8
Experimental matrix.

	Carbon SSA	Batch composition	Situation
Medium SSA carbon	Medium	Medium % CB + EG-1	On test
High SSA carbon	High	Low % CB + EG-1	On test
		Medium % CB + EG-1	On test
Standard for comparison		Standard additives	On test

CB: activated carbon.
EG-1: expanded graphite.

to this, the development of capacitance values similar to the ones of the positive rely almost completely on the addition of very high specific surface area additives such as activated carbon or similar materials.

4.2. Experimental work

All the tests trying to implement supercap effect have been conducted in Spiral wound 6 V 24 Ah modules in which, durations on Power Assist Cycle Life test of 200,000 cycles have been obtained. The idea is then to try to supplement the well proven Spiral wound technology with the supercap effect to eventually move life durations to the range of 300,000 cycles equivalent to 7500 capacity turnover (Table 8).
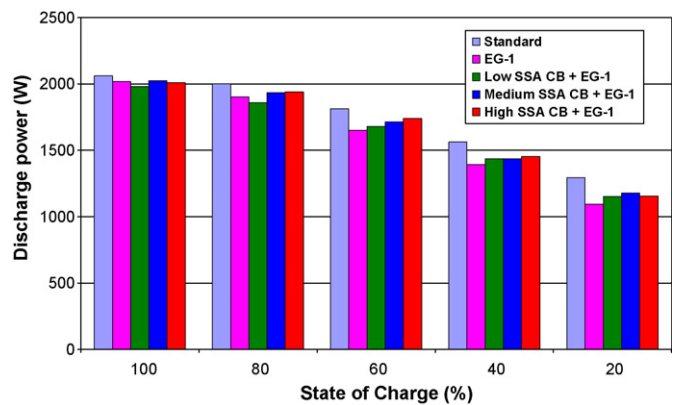
An initial test with intermediate SSA was made in order to gain experience about the mixing process when using high SSA materials. Mixing required extra water addition to deal with the high water absorption of the carbon.

All CB concentrations, include the addition of Expanded Graphite type EG-1 already tested in previous projects, that has revealed as the most effective one. The objective for using expanded graphite is because the electrical specific conductivity of carbons is lower than the one of graphite. It is important not only to achieve very high faradic capacitance, but also to get an as low as possible Equivalent Series Resistance (ESR) of the supercapacitor to allow it to provide as much charge and discharge current during the high rate steps of the Power Assist cycle. Equivalent Series Resistance has also a direct influence on what is called the supercapacitor Time Constant, that is the product of the faradic capacitance and the Equivalent Series Resistance (C*R). It is necessary for this parameter to be relatively large to allow the supercap to take some proportion of the charging current at the end of the 1 C charging period, but it is better to increase the value of the time constant by increasing the faradic capacitance preserving low ESR values (Table 9).

The most remarkable changes in negative plate characteristics are porosity whose value changes from 50 to 54 and 60% when changing from standard to mix with medium and high SSA carbon. As a consequence paste density decreases from the standard value 4.3–3.8 and 3.07 for the corresponding carbon mix. Finally negative AM SSA experiment a marked increase from 2.4 to 3.2 and 6.1 m^2 g^{-1}. Once the battery is electrochemically formed SSA values

Fig. 15. Discharge power, 5 V, 10 s, 25 °C.

are slightly decreased to 1.5 and 4.3 m^2 g^{-1} for medium and high SSA additions.

4.3. Electrical testing

The following table shows the initial performances of all the batches tested in Parts 2 and 3 (Table 10).

Values show no influence in low rate discharges, whereas on high rate low temperature discharges there is a strong effect when adding high SSA carbon. Voltage on discharge falls below the limiting value and consequently discharge duration is heavily affected.

4.3.1. Charge and discharge power
4.3.1.1. Discharge power. The values are represented together to the ones of Part 2 to show the evolution. No noticeable effect is seen for the different additives, with similar values at the different SoC's (Fig. 15).

4.3.1.2. Charge acceptance power. The situation is totally different concerning charge acceptance. A strong influence is observed for the different additives. These big differences are related with the use of carbon, being in direct relation with the SSA of the carbon used. The differences occur at all SoC's but in percentage they are more important for high SoC's, being this fact important, because it would allow to work at a little bit higher SoC, without loosing charge acceptance capability. Charge acceptance values at low SoC (20 and 40%) are in the range 2000–2500 W per module which represents charging currents of the order of 300 A for the modules with the addition of the highest SSA carbon (Fig. 16).

4.3.2. Power Assist Cycle Life
Up to now Power Assist Cycling, has not been completed. Only the group with medium SSA is in an advanced stage, having achieved 160,000 cycles. The other two groups standard and high SSA are in an early stage and hence no conclusion can be derived (Fig. 17).

Table 9
Characteristics of unformed plates.

Batch	Plate	Chemical analysis		Porosimetry			Specific surface area BET (m^2 g^{-1})
		Pb (%)	PbSO$_4$ (%)	Porosity (%)	Apparent density (g cm^{-3})	Median pore diameter (μm)	
Medium SSA CB + EG-1	Positive	2.3	6.3	52.8	4.16	0.29	1.56
	Negative	2.8	6.5	53.9	3.80	0.18	3.21
High SSA CB + EG-1	Positive	0.9	6.5	53.8	4.15	0.26	1.98
	Negative	0.6	6.1	59.9	3.07	0.21	6.08
Standard	Positive	1.6	6.2	51.0	4.35	0.29	1.83
	Negative	1.8	5.9	49.8	4.34	0.18	2.46

Table 10
Initial characterisation.

Reference	Weight	Internal resistance (25 °C, 1 kHz) (mΩ)	C_{20} (1.2A/5.25 V) (Ah)	Reserve capacity (25A/5.25 V) (min)	HR discharge −18 °C (400 A/3.6 V)	
					V_{10s} (V)	$D_{3.6V}$ (s)
EG-1	4.74	2.18 ± 0.05	24.4 ± 0.5	40.9 ± 0.5	4.28 ± 0.03	38 ± 2
EG-2	4.74	2.19 ± 0.03	25.5 ± 0.2	41.3 ± 0.5	4.21 ± 0.01	39 ± 1
EG-3	4.72	2.20 ± 0.04	24.7 ± 0.2	39.6 ± 0.2	4.28 ± 0.02	39 ± 2
SG	4.73	2.23 ± 0.04	24.3 ± 0.3	37.9 ± 1.0	4.16 ± 0.07	31 ± 4
EG-CCB	4.57	2.31 ± 0.07	24.5 ± 0.4	37.4 ± 1.4	4.12 ± 0.04	31 ± 2
Medium SSA CB + EG-1	4.71	2.33 ± 0.06	24.6 ± 0.3	38.4 ± 0.8	4.19 ± 0.07	26 ± 4
High SSA CB + EG-1	4.52	2.41 ± 0.08	25.6 ± 0.6	41.6 ± 1.9	<3.6	7 ± 2
Standard	4.68	2.22 ± 0.07	24.9 ± 0.9	40.3 ± 1.1	4.18 ± 0.07	32 ± 4

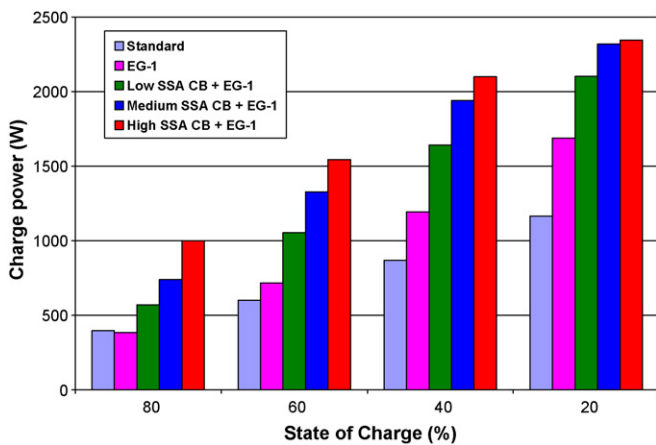### 4.3.3. Tests to simulate supercapacitor effect on charge and discharge

In order to study what would be the influence of supercapacitor implementation inside the battery, a series of tests were made by using commercial supercapacitors externally connected in parallel with the battery, and submitting it to charge and discharge power test at different SoC's. Results can be seen in Figs. 18–20.

4.3.3.1. Discharge power.
The effect of supercapacitor is clearly seen. The current delivered by the combination supercap + battery is higher than the one of the battery alone. This is especially true at the beginning of each discharge period with a sharp increase and subsequent decline.
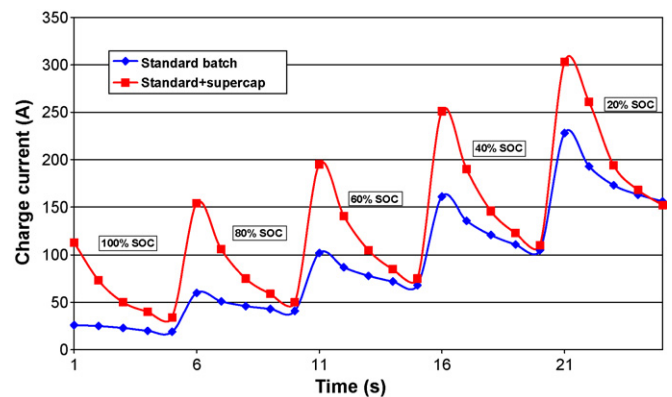
4.3.3.2. Charge acceptance power.
Supercapacitor effect, is even more marked on charge. In this case, the initial current peak that corresponds to the current taken by the supercap, is more important than in discharge. The current decline after the maximum is
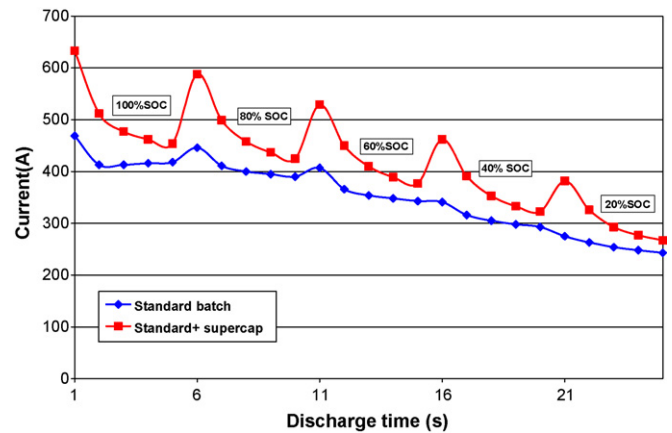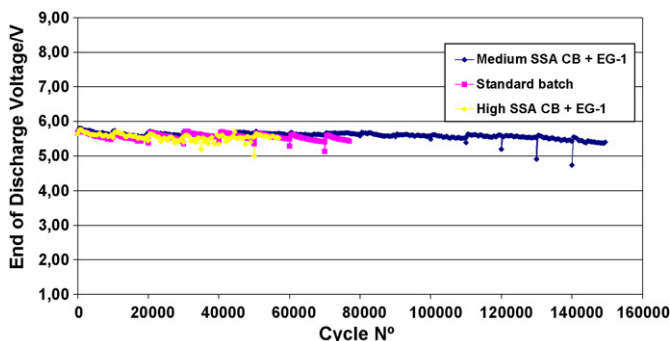

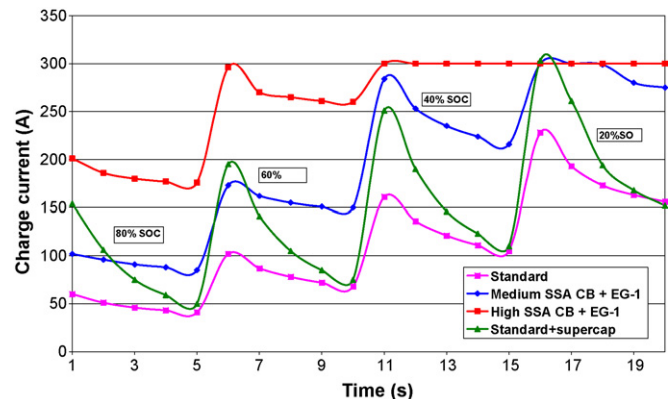**Fig. 18.** 6 V/24 Ah Module + supercapacitor. Discharge power, 5 V, 10 s, 25 °C.

Fig. 19. 6 V/24 Ah Module + supercapacitor. Charge acceptance power, 8 V, 5 s, 25 °C.

Fig. 16. Charge acceptance power, 8 V, 5 s, 25 °C.

Fig. 17. Power Assist Cycle Life test, 60% SoC, 2.5% DoD.

Fig. 20. Negative mix and supercapacitor comparison. Charge acceptance power, 8 V, 5 s, 25 °C.
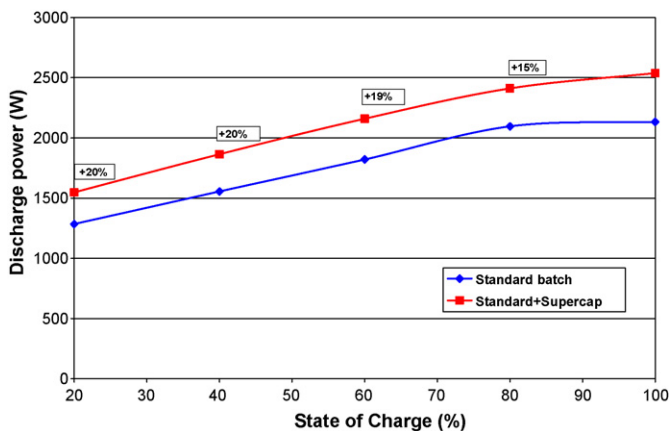
Fig. 21. 6 V/24 Ah Modules and supercapacitor. Discharge power, 5 V, 10 s, 25 °C.

not so sharp as it will be for only the supercap, because the electrochemical charging reactions in the battery begin to take place and contribute progressively more and more to the total charging current.

Possible supercapacitor effect of the carbon formulations tested. In order to ascertain the possible supercapacitor effect brought about by the use of carbon and graphite in the negative mix, all the formulations are compared in the following graph with the combination battery + Supercap.

Comparing the shape of the charging curves, an initial peak that is progressively higher as the SSA of the added carbon increases is observed. This initial peak is more marked as the SoC of the battery decreases. This is an expected fact because the electrochemical charging reactions of the battery contribute less and less as the SoC decreases. These facts indicate that the more probable way of working of the added carbon is through the supercapacitor effect.

4.3.4. Charge and discharge power improvement due to supercapacitor effect

Figs. 21 and 22 show the improvements in both charge and discharge power as a result of having a supercapacitor (52 Farads in this case) in parallel with the battery.

4.3.4.1. Discharge. An increase of between 15 and 20% is observed, being the effect more pronounced as the SoC of the battery decreases.

4.3.4.2. Charge. The effect is by far more pronounced with increments ranging from 18 to more than 100% at high battery SoC's. At
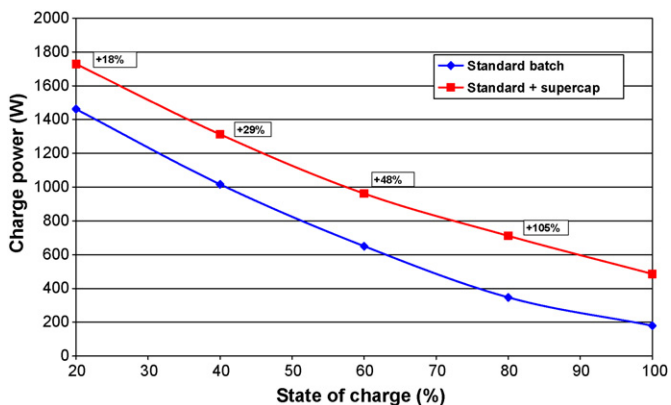

Fig. 22. 6 V/24 Ah Modules and supercapacitor. Charge acceptance power, 8 V, 5 s, 25 °C.

60% SoC a value that typically can be found on hybrid vehicles, the increase is close to 50%. This enhanced charge acceptance by the supercapacitor implementation could be used to eventually having the battery working at higher SoC's in real use, which would be beneficial for battery life.

5. Conclusions

The three different stages in which this work on carbon and graphite in the negative mix has been divided, have allowed to reach a series of conclusions regarding the cause of failure of the negative plate on cycling and the effect of the addition of graphite and carbons of different SSA and conductivity with respect charge and discharge power as well as in Power Assist Cycle Life.

From part 1 it is clear that the cause of negative plate failure is the progressive accumulation of lead sulphate on the structure of the plate with cycling. Lead Sulphate tends to accumulate on the outer part of the plate, forming a strong and dense layer that heavily inhibit the acid diffusion to the reaction pores, as well as creating a high ohmic resistance barrier. This fact, originate strong ohmic drop and polarisation effects due to acid depletion or over-concentration, that strongly reduce the performance on charge and discharge. When graphite or carbon is added, lead sulphate continues to be generated on cycling, but instead of being deposited on the surface, it is evenly distributed all along the thickness of the plate, and in this way it does not represent such an important barrier for acid diffusion, and consequently electrical performance of the battery is greatly increased.

Part 2 shows that even the addition of low SSA graphite and carbon results in a remarkable improvement of both charge acceptance power and cycle life, reaching 200,000–220,000 cycles. When using a combination of low SSA carbon and graphite, charge acceptance is further increased with respect to only graphite, and this fact shows that probably the use of higher SSA carbon could bring about further increases, through the implementation of some degree of supercapacitor effect inside the battery. Power Assist Cycle Life does not show dependence of carbon SSA, obtaining the same cycle life as with negative mix of only graphite.

In part 3, the use of high SSA carbon has resulted in very high values of charge acceptance power that for low battery SoC are in excess of 2000 W for a 6 V module. With respect to the way of working of carbon, from the graph showing comparatively the shape of the charge current of the different mix and the one of the parallel combination of battery plus external supercap, it seems that the most probable mechanism would be internal supercap effect implementation.

The use of carbon in negative mix, has revealed as a broad field of battery development on the hybrid vehicle application, opening the possibility of new and outstanding battery performance improvements that can situate the lead acid battery in an optimum position for its widespread use on hybrid vehicle.

Acknowledgement

References

[1] E. Karden, S. Ploumen, B. Fricke, T. Miller, K. Snyder, Proc. 10th European Lead Battery Conference, Athens, September, 2006.
[2] M. Anderman, J. Power Sources 127 (2004) 2–7.
[3] "Well-to-Wheels Analysis of future automotive fuels and powertrains in the European context", EUCAR Report, November 2003.
[4] E. Karden, P. Shinn, P. Bostock, J. Cunningham, E. Schoultz, D. Kok, J. Power Sources 144 (2005) 505–512.
[5] N. Sato, Proceedings of the 3rd International Advanced Automotive Battery Conference, Nice, June, 2003, Session 3A, paper 11.

[6] P. Reasbeck, J.G. Smith, Batteries for Automotive Use, Research Studies Press Ltd., Baldock, Hertfordshire, England, 1997.

[7] D. Berndt, J. Power Sources 100 (2001) 29–46.

[8] P. Ruetschi, J. Power Sources 127 (2004) 33–44.

[9] P.T. Moseley, D.A.J. Rand, J. Power Sources 133 (2004) 104–109.

[10] S. Fouache, A. Chabrol, G. Fossati, M. Bassini, M.J. Sáinz, L. Atkins, J. Power Sources 78 (1999) 12–22.

[11] S. Fouache, J.P. Douady, G. Fossati, C. Pascon, J. Power Sources 67 (1997) 15–26.

[12] F. Trinidad, F. Sáez, J. Valenciano, J. Power Sources 95 (2001) 24–37.

[13] R.D. Brost, in: D.A.J. Rand, P.T. Moseley, J. Garche, C.D. Parker (Eds.), Valve Regulated Lead-acid Batteries, Elsevier, Amsterdam, 2004, pp. 327–396.

[14] EUCAR Traction Battery Working Group: Specification of test procedures for hybrid electric vehicle traction batteries, September 1998.

[15] J. Valenciano, A. Sánchez, F. Trinidad, A.F. Hollenkamp, J. Power Sources 158 (2006) 851–863.

[16] L.T. Lam, R. Loney, N.P. Haigh, J. Power Sources 174 (2007) 16–29.

[17] B.E. Conway Electrochemical Supercapacitor. Scientific Fundamentals and technological applications. Kluwer Academic Plenum Publisher.